Remote Sensing of Environment 247 (2020) 111911

Contents lists available at ScienceDirect

Remote Sensing of Environment

journal homepage: www.elsevier.com/locate/rse

Influence of surface water on coarse resolution C-band backscatter: Implications for freeze/thaw retrieval from scatterometer data

Helena Bergstedt[a,b,f,*], Annett Bartsch[b,c], Claude R. Duguay[d,e], Benjamin M. Jones[f]

[a] Department of Geoinformatics Z-GIS, University Salzburg, Salzburg, Austria
[b] Austrian Polar Research Institute, Vienna, Austria
[c] b.geos, Korneuburg, Austria
[d] Department of Geography and Environmental Management, Interdisciplinary Centre on Climate Change,University of Waterloo, Waterloo, Ontario, Canada
[e] H2O Geomatics Inc., Waterloo, Ontario, Canada
[f] Institute of Northern Engineering, Water and Environmental Research Center, University of Alaska Fairbanks, Fairbanks, AK, USA

ARTICLE INFO

Keywords:
Freeze/thaw
Surface water
Lake ice
ASCAT
Sentinel-1
SAR

ABSTRACT

The freeze/thaw state of permafrost landscapes is an essential variable for monitoring ecological, hydrological and climate processes. Ground surface state can be obtained from satellite data through time series analysis of C-band backscatter from scatterometer and Synthetic Aperture Radar (SAR) observations. Scatterometer data has been used in a variety of studies concerning freeze/thaw retrieval of the land surface. Coarse spatial resolution scatterometer data has great potential for application in this field due to its high temporal resolution (approx. daily observations). In this study, we investigate the influence of sub-grid cell (12.5 km) surface water (ice free and ice covered) on freeze/thaw retrieval based on ASCAT data using a threshold algorithm. We found discrepancies related to the surface water fraction in the detected timing of thawing and freezing of up to 2 days earlier thawing for spring and 3.5 days earlier freezing for autumn for open water fractions of 40% resulting in an overestimation of the frozen season. Results of this study led to the creation of a method for correction of water fraction impact on freeze/thaw data. Additionally, this study demonstrates the applicability of a new approach to freeze/thaw retrieval which has not so far been tested for SAR, specifically Sentinel-1.

1. Introduction

Lakes and lake-rich landscapes are a dominant and highly variable feature in the Arctic (Duguay et al., 2002; Lehner and Döll, 2004; Smith et al., 2007; Grosse et al., 2013). These lakes of different shape, size and depth are complex systems of water bodies, influencing surrounding landscapes evolution and shaping landscape ecology (Smith et al., 2007; Grosse et al., 2013). In remote sensing studies, lakes and other water bodies (*e.g.* ponds, rivers) often impact the retrieval of geophysical parameters such as soil moisture (*e.g.* Högström et al., 2014), snow water equivalent (*e.g.* Rees et al., 2006; Kontu et al., 2008; Green et al., 2012) and vegetation indices (*e.g.* Jiang et al., 2006). In particular, lakes of sub-pixel size can lead to misclassification or errors in the Earth observation results, causing problems in both coarse scale optical (*e.g.* Bartsch et al., 2016) and microwave remote sensing (Högström et al., 2014; Högström and Bartsch, 2017). However, remote sensing has also been directly applied to study lakes and their features in numerous studies ranging from water quality retrieval (Kutser et al., 2016) to quantifying surface water dynamics (Carroll et al., 2016; Nitze et al., 2018), water storage (Cai et al., 2016) and size distribution (Polishchuk et al., 2017).

Next to the abundance of lakes, permanently frozen ground is a characterizing feature of Arctic landscapes. In the Arctic, the landscape is underlain by perennially frozen ground known as permafrost. Following temperature changes in spring and autumn, the ground surface undergoes an annual thaw/freeze cycle. Transitional periods are characterized by partially frozen and thawed landscapes (Frauenfeld et al., 2007) as well as daily thawing and refreezing in connection with air temperature variations (Bartsch et al., 2007). These thawing and freezing cycles have been linked to a multitude of hydrological processes including surface runoff (Wang et al., 2009), ground water movement (Woo and Winter, 1993), infiltration and evapotranspiration (Arp et al., 2015; Woo, 1986) as well as mean annual ground temperature (Arp et al., 2016; Kroisleitner et al., 2018) and ground surface deformation (Bartsch et al., 2019). In addition, the thawing and refreezing of the ground is known to influence methane emissions

* Corresponding author at: Department of Geoinformatics Z-GIS, University Salzburg, Salzburg, Austria.
E-mail address: hbergstedt@alaska.edu (H. Bergstedt).

https://doi.org/10.1016/j.rse.2020.111911
Received 9 September 2019; Received in revised form 15 April 2020; Accepted 20 May 2020

(Mastepanov et al., 2008; Arndt et al., 2019) and has been found to have a significant impact on terrestrial carbon exchange (Schuur et al., 2008). The Arctic and its permafrost dominated landscapes are known to be highly affected by climate warming, with temperatures in these regions rising faster compared to lower latitudes (Pithan and Mauritsen, 2014). Under warming conditions the extent of permafrost as well as seasonal frost effects and thawing and refreezing cycles are expected to change (Zhang et al., 2008; Romanovsky et al., 2015).

Mapping frozen and thawed ground and detecting the timing of the surface state change is therefore crucial for climate models as well as hydrological and ecological applications (Zhang et al., 2004). Microwave remote sensing has been used in the past to monitor the surface state of permafrost areas (Zhang and Armstrong, 2001; Kim et al., 2011; Naeimi et al., 2012; Kimball et al., 2004; McDonald and Kimball, 2006). Backscatter values vary due to changes in the dielectric constant of the water contained within the upper part of the ground (Dobson and Ulaby, 1986; Ulaby et al., 1978), which changes significantly when the soil water freezes (Wegmüller, 1990). At C-band (5.3 GHz) this leads to overall lower backscatter during the frozen period compared to the unfrozen period (*e.g.* Rignot and Way, 1994; Duguay et al., 1999; Park et al., 2011). The absolute difference between backscatter values during frozen and thawed conditions varies for sites with different surface characteristics. For example Naeimi et al. (2012) found differences in winter and summer mean backscatter of approximately 1.5 db to 3 db for sites covered with wooded tundra, differences of approximately 2 db for herbaceous tundra and approximately 3 db for sites with broadleaved forest. Several algorithms using both scatterometer and Synthetic Aperture Radar (SAR) data to detect the timing of freezing and thawing of the ground surface, relying on the difference of winter and summer backscatter, have been developed in the past (Naeimi et al., 2012; Park et al., 2011; Derksen et al., 2017; Kimball et al., 2001).

Freeze/thaw data products have been derived from different sensors (active as well as passive systems) utilizing different frequencies as well as temporal and spatial resolutions (Kim et al., 2017; Naeimi et al., 2012; Paulik et al., 2014; Sabel et al., 2012; Derksen et al., 2017; Rautiainen et al., 2016). To this date, only a few studies utilized Sentinel-1 data for freeze/thaw retrieval (*e.g.* Baghdadi et al., 2018). In the creation of freeze/thaw products (*e.g.* Paulik et al., 2014), lake masks are typically applied to avoid errors in the classification due to the influence of water bodies. Backscatter of surface water is known to be different compared to the surrounding land areas and can be influenced by different processes. During the ice free months, wind is a known influence, changing the surface roughness of the water bodies which leads to a different backscatter (Duguay et al., 1999; Högström et al., 2014). While the ground surface thaws in spring and freezes in autumn, ice break-up and freeze-up takes place on lakes. Remote sensing of lake-ice break-up and freeze-up has been the subject of a few studies in the past (*e.g.* Surdu et al., 2015; Arp and Jones, 2009). In the period during which the soil is frozen, the backscatter of lakes can be influenced by ice cover being frozen to the ground (called ground fast ice) or floating which leads to differing backscatter responses (Duguay et al., 1999, 2002; Bartsch et al., 2017a, 2017b; Pointner et al., 2018; Engram et al., 2018). During spring time, a lag between the thawing of the ground surface and lake ice occurs where the terrestrial landscapes are thawed but lake surfaces are still covered by a decaying ice cover. This leads to a period in time, of up to several weeks, where the backscatter signal is impacted by frozen lakes and thawed ground surfaces.

When using microwave remote sensing data both options, scatterometer and SAR data, have particular advantages and disadvantages specific to each data type. Scatterometer data has the advantage of high temporal resolution, providing approximately daily observations, allowing for the monitoring of short term processes and changes. SAR sensors provide data in a higher spatial resolution (up to 20 m for Sentinel-1), however data products based on SAR generally suffer from the low temporal resolution of the SAR observations. SAR data, like Sentinel-1 as well as previous sensors, have been used to assess spatial variability and the validity of scatterometer observations. Pathe et al. (2009) derive soil moisture with data obtained from the Advanced Synthetic Aperture RADAR (ASAR) sensor onboard the ENVISAT satellite. A comparison of the results with 50 km soil moisture data from the European Remote Sensing Satellite (ERS) showed the capability of SAR data to resolve spatial patterns in soil moisture that are omitted by scatterometers (*e.g.* differences in soil moisture due to different vegetation covers). Högström et al. (2014) and Högström and Bartsch (2017) use data from ASAR to assess backscatter variations over water bodies with regard to soil moisture derived from measurements of the Advanced Scatterometer (ASCAT) onboard the MetOp satellites. Bauer-Marschallinger et al. (2018) use Sentinel-1 and ASCAT derived surface soil moisture products to create a product with both high temporal and spatial resolutions. The authors use data fusion methodologies to overcome the inherent problem of coarse scatterometer data and low temporal resolution of the SAR observations. ASAR was also used to study the spatial variability of soil freezing and thawing within a scatterometer footprint (Bergstedt and Bartsch, 2017). Lake-rich areas have been confirmed to have the largest influence on scale discrepancies outside of mountainous terrain. The impact on the accuracy of surface state retrieval has so far not been quantified.

The objective of this study is to assess and quantify the impact of sub-grid cell water bodies on the backscatter signal of a scatterometer sensor (ASCAT) using SAR (Sentinel-1) backscatter time series with regard to freeze/thaw retrieval from coarse resolution scatterometer data. We hypothesize that the surface water fraction on a sub-grid cell scale influences the quality of the detected freeze/thaw timing by influencing the backscatter level. The chosen study sites are situated in Alaska, northern Canada and Europe, and encompass a wide range of open water fractions. We present a quantification of the temporal offset in the detected freeze/thaw timing as retrieved from coarse scale scatterometer time series caused by sub-grid cell surface water. The results of this study have implications for future improvements in freeze/thaw applications.

2. Study sites and data sets

2.1. Study sites selection

To analyze the influence of the sub-grid cell open water fraction on backscatter time series of ASCAT, we chose multiple study sites in Alaska, northern Canada and Finland (see Fig. 1). For most study sites, several ASCAT grid cells were chosen to increase the representativeness of the results increasing the number of studied grid cells to 50. Study sites were chosen to represent areas in the low and high Arctic as well as for different lake sizes and fractions (see Fig. 2). The open water fraction of the study sites varies between 1% and 60%. The extent of study sites was chosen on the basis of the 12.5 km grid of ASCAT data. The overall studied time period is 01/2015 to 10/2018, and limited by the availability of Sentinel-1 observations for each specific study site.

2.2. MetOp ASCAT data

The scatterometer data used in this study was obtained from the Advanced Scatterometer (ASCAT) instrument on board the MetOp satellites. The ASCAT instrument operates at C-band (5.255 GHz) and provides up to daily coverage of our study sites since 2007 (Figa-Saldaña et al., 2002) (Table 1). The ASCAT time series (backscatter, sigma naught (σ^0)) were extracted from the database provided by the European Organisation for the Exploitation of Meteorological Satellites (EUMETSAT) and are part of the soil moisture product series (data product ASCAT Soil Moisture at 12.5 km Swath Grid–Metop). The data product used for this analysis are provided with 25 km resolution gridded to 12.5 km (Figa-Saldaña et al., 2002). The data is provided normalized to an incidence angle of 40° (Naeimi et al., 2009).

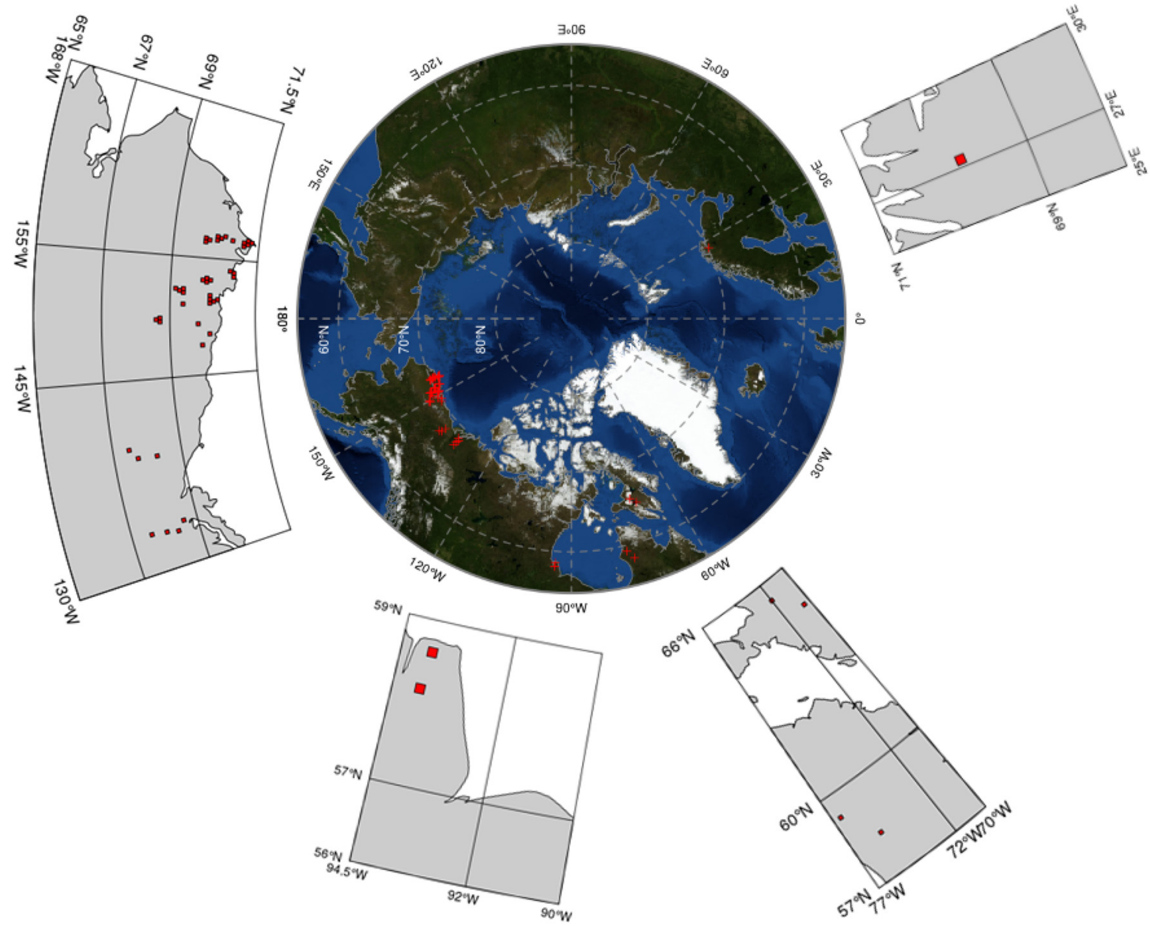

Fig. 1. Circumpolar and zoomed in views of the locations of all 50 study sites included in this analysis (Background map: Blue Marble: Next Generation, NASA Earth Observatory). (For interpretation of the references to colour in this figure legend, the reader is referred to the web version of this article.)

2.3. Sentinel-1 synthetic aperture radar data

The Sentinel-1 radar Earth observation mission is part of the Copernicus Programme (Geudtner et al., 2014). It consists of two satellites (Sentinel-1A and 1B) that were launched in April 2014 and April 2016, respectively. The data from Sentinel-1 provides a higher spatial resolution (5 × 5 m to 20 × 50 m) at C-band (5.405 GHz) compared to most previous systems and scatterometer missions since 2014 (Showstack, 2014). The SAR data from Sentinel-1 was obtained through the Copernicus Open Access Hub. Sentinel-1 data used in this study was acquired in the Interferometric Wide swath (IW) mode in VV-polarization (20 × 22 m spatial resolution, 10 × 10 m pixel spacing) (Table 1). Available Sentinel-1 data in VH-polarization was not considered as there is no corresponding equivalent for ASCAT. To maximize the number of observations, data from both descending and ascending overpasses were included. The relative orbits for Sentinel-1 included for the different study sites are reported in Table 2.

2.4. Multispectral Sentinel-2 satellite imagery

To distinguish the lakes in the grid cells from the surrounding land areas we created lake masks using cloud free Sentinel-2 optical satellite

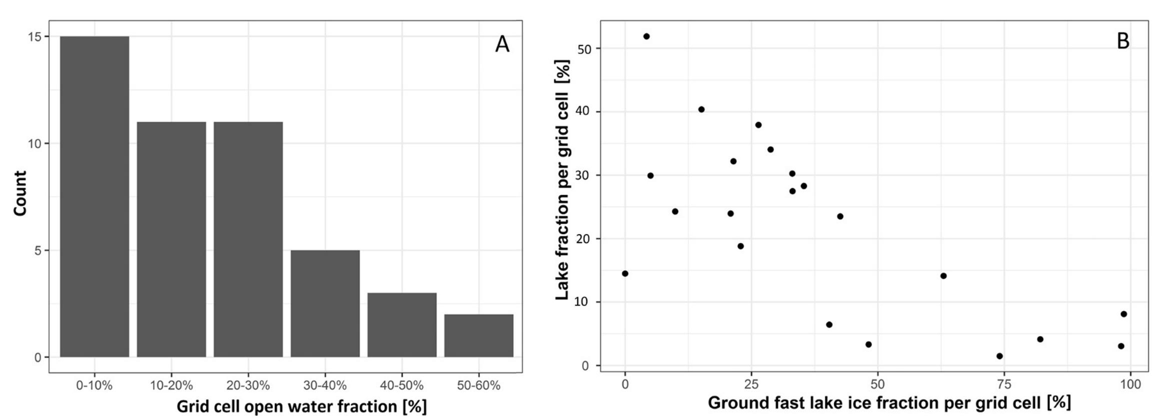

Fig. 2. Characteristics of studied grid cells: (A) Count of study site grid cells with respective open water fractions and (B) overall open water fraction *vs.* fraction of lakes with ground fast ice occurring during the frozen period (Bartsch et al., 2017a, 2017b).

Table 1
Specifications of remote sensing data sets used in this study, including the Advanced Scatterometer (ASCAT), Sentinel-1 and Sentinel-2. The temporal resolution indicated in the table is valid for time periods after the launch of Sentinel-1b and Sentinel-2b. Data availability (for observations covering our study sites) is given in months and years.

Sensor	Specification	Spatial resolution	Temporal resolution	Data availability
ASCAT	C-band, VV-pol.	25 km (12.5 km grid)	~ daily	01/2007–ongoing
Sentinel-1	C-band, VV-pol. Interferometric Wide swath (IW) mode	20 × 22 m (10 m pixel spacing)	~ 3 days	01/2015–ongoing
Sentinel-2	Multi-spectral	10 m - 60 m	~ 5 days	06/2015–ongoing

imagery. Sentinel-2 is an optical high-resolution Earth observation mission and part of the Copernicus Program (Gascon et al., 2014). Currently it consists of two satellites (Sentinel-2A and 2B) which have been launched in June 2015 and March 2017, respectively. Both satellites are orbiting Earth in a polar, sun-synchronous orbit providing multispectral data in 13 spectral bands with a spatial resolution of 10 m to 60 m (Gascon et al., 2014). The Sentinel-2 data used in this study is Level 1C data, providing top of atmosphere reflectances (Gascon et al., 2014) (see further details in Table 1).

2.5. ERA-interim temperature data

The temperature data used in this study was obtained in large parts from the ECMWF ReAnalysis (ERA-Interim) data set which is provided by the European Centre for Medium-Range Weather Forecasts (ECMWF). This data set provides global coverage of temperature data and is based on the ECMWF Integrated Forecast Model. The data set contains air temperature as well as surface temperature information from 1989-present (Dee et al., 2011). This study used soil temperature of the surface level (0–7 cm) for the determination of different backscatter levels (Naeimi et al., 2012).

2.6. In situ data

In situ data consisting of soil and lake temperature measurements, used to support the analysis of satellite observations, were available for a limited number of sites, located in northern Alaska and northern Finland (see Table 2). These data sets were gathered through different networks. Transmitted C-band radar signals have been found to penetrate into the ground up to 5 cm (*e.g.* Matgen et al., 2012; Naeimi et al., 2012) and the penetration depth is known to increase up to 9 cm when the ground is frozen (Wegmüller, 1990; Zhao et al., 2012). Additionally, penetration depth is known to vary depending on soil moisture (Ulaby et al., 1996). In this study, we included soil temperature observations of the upper 30 cm to account for the variability of the penetration depths and to maximize the number of available *in situ* measurements. In total, 5 of the chosen grid cells contained one or more *in situ* measurement sites with suitable observations during the time frame limited by the availability of Sentinel-1 data (since 2015). Two grid cells located in Barrow and the Deadhorse areas both contain three observation sites each with data provided by the Permafrost Laboratory (www.permafrost.gi.alaska.edu). Data included near-surface soil temperature and, in a more limited way, volumetric water content measured at different depths. Grid cell 3080728 contains observation sites from the Circum-Arctic Lake Observation Network (CALON). For one of the sites (Teshekpuk Lake), lake bed and lake surface temperature was available for part of the studied time frame (12/2015–10/2017). For more detailed information on the measurement set up for the CALON sites see Arp et al. (2015, 2016). For grid cell 3061839 located in northern Finland, near surface soil ground temperature measurements were available for the years 2016–2018. Temperature measurements were obtained by distributing iButton temperature loggers to cover different landscape types and different elevations within the grid cell. The iButton loggers were placed approximately 2–3 cm below the surface to avoid direct warming influence by the sun. Temperature data for the Kaldoaivi site can be obtained from the PANGAEA data repository (Bergstedt and Bartsch, 2020).

2.7. Additional data sets

A data set consisting of the ground fast lake ice fraction (Bartsch et al., 2017a, 2017b) was used to compare the results of our analysis with the ground fast lake ice fraction of the study sites. The ground fast lake ice fraction data set was created based on ENVISAT ASAR Wide Swath data and published as a supplement to Bartsch et al. (2017a, 2017b). The data set is based on circumpolar ASAR observations from late winter 2008.

To compare our lake mask with established data products, we utilized the Global Surface Water (GSW) Water Occurrence data set (Pekel et al., 2016) which contains the frequency with which water was present at the surface between 1984 and 2018 for any given area. To compare our water mask to a data product geared towards Arctic applications, we utilized the Permafrost Region Pond and Lake data base (PeRL) (Muster et al., 2017). This data set is based on high resolution

Table 2
Overview of all *in situ* data sets used in this study, including the respective ASCAT grid cell, the site name, date range used in this study, observed variable (soil temperature, lake surface temperature, lake bed temperature) and relative Sentinel-1 orbits used for each ASCAT grid cell. Deadhorse and Barrow data sets were obtained from the Permafrost Laboratory, Data sets for grid cell 3080728 were obtained through the Circum-Arctic Lake Observation Network (CALON) (TLO: Teshekpuk Lake Observatory).

ASCAT grid Cell	Location	Site	Variable	Date range	Rel. S1 Orbits
3061839	69.83°N, 27.27°E	Kaldoaivi	Soil temp.	09/2016–07/2018	14, 43, 51, 116, 124, 153
3069922	70.09°N, 148.58°W	Deadhorse 2	Soil temp.	12/2016–07/2017	95, 102, 123, 131
	70.10°N, 148.59°W	Deadhorse 3	Soil temp.	12/2016–07/2017	
	70.10°N, 148.58°W	Deadhorse 4	Soil temp.	12/2016–07/2017	
3080728	70.75°N, 153.86°W	Tes005	Lake bed & lake surf. temp.	12/2015–10/2017	65, 73, 94, 102, 138
	70.70°N, 153.92°W	Tes006	Lake bed & lake surf. temp.	12/2015–10/2017	
	70.72°N, 153.83°W	TLO	Soil temp.	12/2015–10/2017	
	71.31°N, 156.66°W	Barrow 2	Soil temp.	01/2017–09/2017	36, 44, 65, 73
	71.28°N, 156.61°W	Barrow A Soil Pit	Soil temp.	01/2017–09/2017	
	71.28°N, 156.60°W	Barrow C Soil Pit	Soil temp.	01/2017–09/2017	

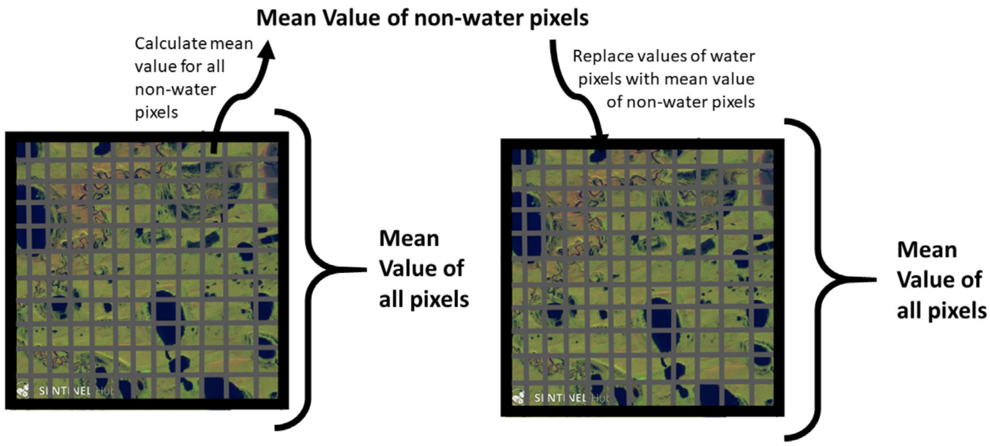

Fig. 3. Schematic of simulating the absence of lakes for lake rich footprint on the scale of 12.5 km ASCAT grid cells using Sentinel-1 SAR data.

aerial and satellite imagery from 2002 to 2013 and includes historical imagery from 1948 to 1965.

3. Methodology

This section describes the methodology and workflow used in this study. The analysis involved optical imagery (Sentinel-2), scatterometer data (ASCAT) and SAR observations (Sentinel-1). Sentinel-1 SAR data was used to assess the impact of sub-grid cell surface water on scatterometer backscatter. To distinguish surface water from land areas, Sentinel-2 water masks were employed.

3.1. Creating lake masks using the normalized difference water index

Lake masks were created using cloud-free Sentinel-2 imagery from the summer of 2016 (June 2016–August 2016) for all areas. To map the waterbodies in each ASCAT grid cell, we calculated the Normalized Difference Water Index (NDWI) following the method described in Du et al. (2016). The NDWI was first proposed by McFeeters (1996) and is calculated as follows

$$NDWI = \frac{\rho_{Green} - \rho_{NIR}}{\rho_{Green} + \rho_{NIR}} \tag{1}$$

where ρ_{Green} and ρ_{NIR} are top of atmosphere reflectance values of the green and near infrared (NIR) bands respectively. Applied to Sentinel-2 this results in

$$NDWI_{10} = \frac{\rho_3 - \rho_8}{\rho_3 + \rho_8} \tag{2}$$

Lakes were identified using an NDWI threshold specific for each site. Given the spatial resolution of Sentinel-2, the resulting NDWI has a spatial resolution of 10 m ($NDWI_{10}$).

3.2. Processing of Sentinel-1 imagery

To allow for an extensive analysis, all usable Sentinel-1 scenes with VV-polarization for the chosen study areas were included into this study. Observations included all time periods (frozen and unfrozen conditions). The Sentinel-1 scenes were pre-processed using the calibration and terrain correction tools of the Sentinel Application Platform (SNAP) software. For the terrain correction we used the Global Earth Topography and Sea Surface Elevation at 30 arc sec resolution (GETASSE) digital elevation model as it is available for all chosen sites. As the incidence angle is known to have a major effect on the backscatter values of SAR imagery, all chosen scenes were normalized using the local incidence angle. Using

$$\sigma^0(40°) = \sigma^0(\theta) - k * (\theta - 40°) \tag{3}$$

where θ is the local incidence angle backscatter values were normalized to a common incidence angle of 40° (Hahn et al., 2017). The parameter k is dependent on the local incidence angle and the corresponding backscatter values and can be derived as follows (Widhalm et al., 2018):

$$k = \frac{(\sigma^0(\theta) - \sigma^0(40°))}{\theta - 40°} \tag{4}$$

To ensure consistency and comparability of the ASCAT and Sentinel-1 results we used the values for the parameter k as provided together with the ASCAT backscatter values by EUMETSAT. To allow for direct comparison with the ASCAT backscatter values, subsets of the Sentinel-1 imagery of the extent of the chosen ASCAT grid-cells were created.

3.3. Comparison of ASCAT and Sentinel-1

In order to have comparable ASCAT and Sentinel-1 time series, we based our analysis on the 12.5 km grid of the ASCAT data set. Sentinel-1 data was subset to match the grid of the ASCAT data. ASCAT data is not originally given in a gridded format but rather each ASCAT observation represents an elliptical footprint. To efficiently compare the SAR and scatterometer time series, an approximation of shape must be made. We chose to subset the Sentinel-1 data to a grid based on the WARP5 grid from the Technical University Vienna (Bartalis et al., 2006; Hahn et al., 2017) using a rectangular approximation. Previous studies have used different shapes to subset SAR data. While some studies have used rectangular grids similar to our approach (Pathe et al., 2009), other studies have used hexagonal (Högström et al., 2014) or circular grids (Bauer-Marschallinger et al., 2018). We limited our analysis to Sentinel-1 data with VV-polarization as this is also the polarization of the ASCAT sensor. From the subsets of Sentinel-1 data, mean values were calculated for each scene considering all pixels, taking into account only those pixels of water body areas as well as considering only those pixels of land areas. To quantify the influence of the water areas on the overall backscatter of each footprint, the values of water pixels were then replaced by the mean value of land pixels and an additional overall mean value was calculated from those rasters (see Fig. 3). Subsequent analyses were done on time series comprised of these mean values.

3.4. Freeze/thaw algorithm

Several algorithms to detect the ground surface state have been developed in the past (*e.g.* Naeimi et al., 2012; Park et al., 2011). Naeimi et al. (2012) present an algorithm designed to retrieve surface state information from ASCAT backscatter data. We based our analysis on their presented algorithm and applied it subsequently to ASCAT backscatter and Sentinel-1 time series. The algorithm is centered on

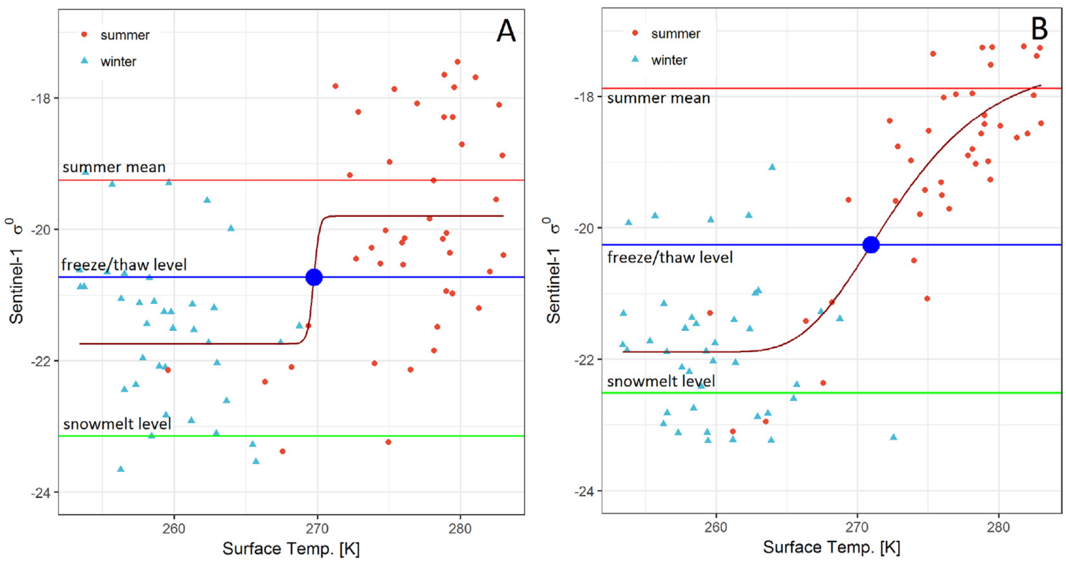

Fig. 4. Example of backscatter *versus* ERA interim reanalysis temperature data for Sentinel-1 time series including (A) and excluding (B) water pixels for one grid cell (70.72°N, 156.69°W) on the Alaskan North Slope. Red curve indicates the best fit logistical function fitted to the Sentinel-1 backscatter. The blue point indicates the inflection point of the fitted logistic function which is assumed to represent the backscatter of the freeze/thaw level. (For interpretation of the references to colour in this figure legend, the reader is referred to the web version of this article.)

finding a threshold for backscatter values, below which the ground surface can be classified as frozen ($\sigma^0 FTL$) (Naeimi et al., 2012). This is achieved by fitting a logistic curve into the backscatter values with respect to temperature around the freezing point. An example of this is shown in Fig. 4. Additionally to the backscatter level of the freeze/thaw level, the algorithm relies on the mean backscatter during the summer months ($\sigma^0 SM$) as well as the backscatter at the snowmelt level ($\sigma^0 SML$). Naeimi et al. (2012) have reported the best results of this process if the regression is limited to values between +10 °C and − 10 °C. This approach has been reported to be applicable for Arctic regions (Naeimi et al., 2012). We determined the three different backscatter levels ($\sigma^0 FTL$, $\sigma^0 SM$, $\sigma^0 SML$) for the overall mean value and the mean value with replaced water pixel values. To assess the influence of water areas on the overall backscatter of the respective ASCAT grid cell, we determined the difference between those backscatter levels relevant for the ASCAT freeze/thaw algorithm for the different Sentinel-1 mean value time series.

To quantify the impact of our findings on the results of the chosen freeze/thaw algorithm, we applied the algorithm as presented in Naeimi et al. (2012) to the created Sentinel-1 time series. The results were analyzed regarding the differences arising from using the different Sentinel-1 time series and we calculated the days per year for which the results showed disagreement.

4. Results

The validation of the surface water mask used in this study using established data sets revealed high agreements. This included a comparison with the Global Surface Water Occurrence data set which shows 96.2% to 96.6% agreement with our Sentinel-2 based water mask. Comparing our mask to the PeRL data base lake inventory shows an agreement of 86.7%.

Fig. 5 shows the difference between Sentinel-1 time series including and excluding lake areas for all 50 selected study sites for all studied years from the launch of Sentinel-1 (Spring 2014) to September 2018. The offset between the two time series is largely positive with mean values close to 0 db during the frozen season, meaning higher backscatter values for the time series including the lake areas, and largely negative for the thawed period, meaning higher backscatter values for the time series excluding lake areas. The variability of the offset is visibly stronger and the absolute values for the offset are higher during the thawed period.

Fig. 6 shows the relationship of differences between backscatter levels ($\sigma^0 FTL$, $\sigma^0 SM$, $\sigma^0 SML$) for Sentinel-1 time series including and excluding open water areas and the open water fraction of the respective ASCAT grid cells. All three differences of backscatter levels show positive Pearson correlations with the open water fraction. The strongest correlation is exhibited by the difference between the summer mean backscatter value (0.879), followed by the correlation of differences between the snow melt backscatter levels (0.691) (see Fig. 6) and the correlations for the differences for backscatter at the freeze/thaw level (0.602) (see Fig. 6). Winter mean values are not significantly different between the time series including and excluding water pixels (see Fig. 7). The correlation of the difference of the ASCAT backscatter at the freeze/thaw level and the lake-excluding Sentinel-1 backscatter at the freeze/thaw level shows a correlation of −0.379 (see Fig. 6).

The findings for differences in timing for thawing and freezing as resulting from the freeze/thaw algorithm when applied to the mean value Sentinel-1 time series including and excluding lakes can be seen in Fig. 8. Applying the freeze/thaw algorithm to the different Sentinel-1 mean value time series results in offsets of up to 4 days per year for thaw timing and up to 5 days per year for freeze-up timing. Fig. 8 shows that this offset created by including lake areas in the analysis leads to an early detection of thaw in spring and a early detection of freeze-up in autumn for the majority of study sites. The offsets in days per year correlate with the open water fraction of the corresponding grid cell with values of 0.837 for thaw and 0.82 for freeze-up. Fig. 8 shows four outliers for the relationship of the offset and the open water fraction regarding the thaw timing and two outliers regarding the freeze-up timing. The outliers represent grid cells types coast, lake and floodplain.

Fig. 9 shows the relationship of the difference in thaw and freeze-up timing in days per year with the fraction of lakes with ground fast ice per grid cell. Comparing the offset to the ground fast lake ice fraction for the corresponding grid cell gives weaker correlations than the analysis considering the general open water fraction (see Fig. 9). For both the thaw timing as well as the freeze-up timing, the correlations are negative. As in Fig. 8, Fig. 9 also shows outliers regarding the thaw and freeze-up timing. Rivers were removed in the ground fast lake ice data set (Bartsch et al., 2017a, 2017b) and those grid cells are therefore not considered in this comparison.

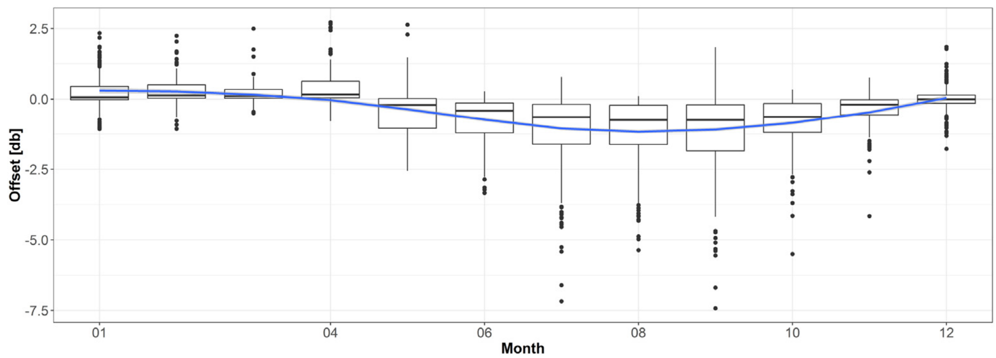

Fig. 5. Offset (in db) for months of the year of the Sentinel-1 time series for all 50 study sites including lakes *vs.* excluding lakes.

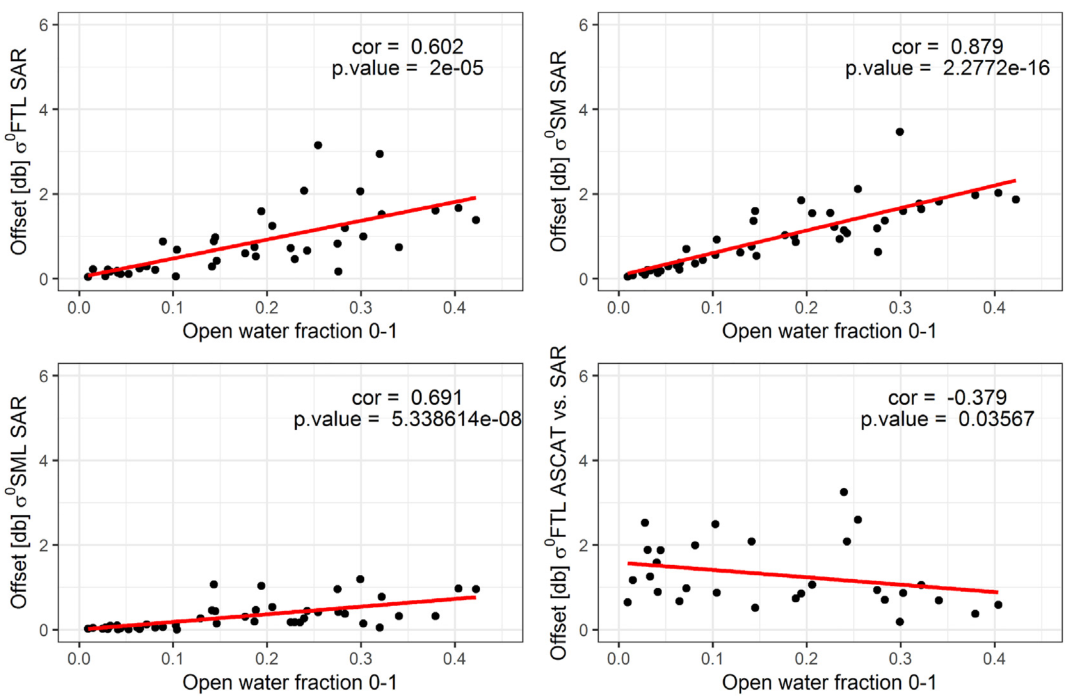

Fig. 6. Offsets in db for time series comprised from different Sentinel-1 mean values (including and excluding lake areas) for three different backscatter levels ($\sigma^0 FTL$, $\sigma^0 SM$, $\sigma^0 SML$) and ASCAT ($\sigma^0 FTL$); FTL - Freeze-Thaw Level, SM - mean of summer months, SML - Snow Melt Level (as defined in Naeimi et al. (2012)).

Figs. 10, 11 and 12 show a comparison of ASCAT and Sentinel-1 time series with *in situ* measurements from the respective grid cells. All three examples show general agreement of the *in situ* measurements and the backscatter, but also the variability of freeze/thaw timings within one grid cell.

To quantify the agreement of the Sentinel-1 freeze/thaw classification with *in situ* near-surface soil temperature measurements we compared the classification results with measurements from 3 different study sites described in Table 2. The agreement of the classification with the *in situ* data records is summarized in Table 3.

5. Discussion

5.1. Influence of unmasked water bodies on freeze/thaw algorithms

Our analysis confirms the significant impact of sub-grid cell water bodies on C-band backscatter. The results are specific to approaches concerning threshold algorithms as proposed by Naeimi et al. (2012). The threshold algorithm used in this study relies on the different backscatter levels during frozen and unfrozen periods. These backscatter mechanisms are disturbed by the presence of sub-grid cell water bodies.

With the exception of windy conditions, open water has low backscatter while ice typically has high backscatter values. Water within the grid cell therefore lowers the overall backscatter during the unfrozen period and increases the backscatter during the frozen periods. This alters the inflection point of the fitted function and thus the location specific threshold for surface state determination.

The offset for the thresholds is strongest for the summer mean (unfrozen period, SM) (see Fig. 6). These results are in good agreement with previous work by Högström et al. (2014) who found low agreement of ASCAT derived soil moisture with model results in areas with high lake fractions. Högström et al. (2014) argue that this is due to wind influencing the backscatter of the surface water areas. Högström and Bartsch (2017) found that a water fraction greater than 20% causes a bias of more than 10% relative surface soil moisture derived from ASCAT data. The authors used wind speed and precipitation data from the harmonized CPC Global Summary of the Day and Month Observations data set. It could be shown that the bias in ASCAT derived soil moisture related to open surface water could be explained best by wind speed observations. The stronger influence of lake areas on the overall backscatter on the grid cell level can also be seen in Fig. 5. Stronger offsets during the thawed periods as well as stronger variability of offsets during this time are evident. The thawed period also shows more

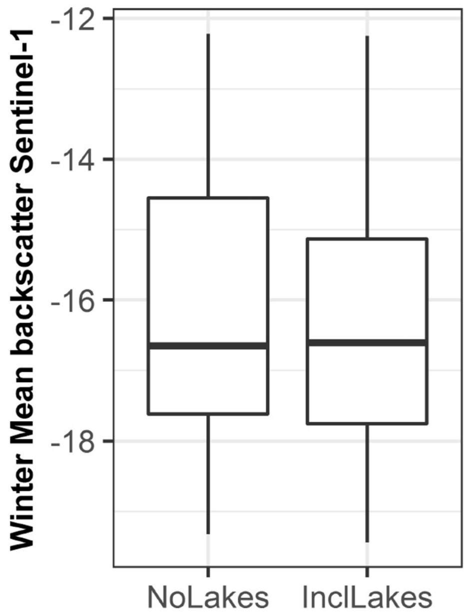

Fig. 7. Sentinel-1 winter mean backscatter values for time series including and excluding water pixel.

outliers of offsets compared to other times. For grid cells without the influence of sub-grid cell water bodies backscatter during summer is higher compared to frozen periods.

Besides the summer mean threshold, other values important for freeze/thaw algorithms include the snowmelt level and the freeze/thaw level (for further explanation see Fig. 4). The offsets for the freeze/thaw level show a weaker correlation with the open water fraction (0.602) compared to the offsets for summer mean and snowmelt level (see Fig. 6). The weaker correlation suggests that the threshold for the freeze/thaw level is comparatively more strongly influenced by other factors such as soil type, soil moisture and vegetation/landcover compared to the influence of the open water fraction. It is therefore a reasonable assumption that those factors also influence the quality of the freeze/thaw level determination. While the correlation of the offset for the freeze/thaw level is less pronounced compared to that of the other parameters (summer mean, snowmelt) the offsets reach up to 4 db, showing that the open water fraction has a strong influence on the backscatter level during thaw and freeze-up for many of the study sites. A comparison of winter mean values shows no significant differences between the time series excluding and including water pixel (see Fig. 7). Previous studies found differences in winter ASCAT backscatter between continuous and non-continuous permafrost sites (Bergstedt et al., 2018). Soil moisture is known to influence the freeze-up process and the intensity of the change in backscatter during the freeze-up process (Hallikainen et al., 1984; Duguay et al., 1999; Naeimi et al., 2012). Naeimi et al. (2012) describe vegetation as one of the factors influencing backscatter in a way that is relevant for freeze/thaw detection. It has been shown previously, that the landscape type influences the results of freeze/thaw algorithms when comparing SAR and scatterometer scales (Bergstedt and Bartsch, 2017). The presence of vegetation is also known to influence the backscatter response at snowmelt (Frolking et al., 1999). Park et al. (2011) show that the thaw date is correlated differently to snow melt depending on the vegetation type. The snowmelt level shows a relatively strong correlation (0.691) with the open water fraction (see Fig. 6). While strongly correlated with the open water fraction, the difference in influence of melting snow on the backscatter level is low with a majority of sites showing offsets under 1 db.

The results in Fig. 8 demonstrate strong relationships for the difference in freeze/thaw timing between Sentinel-1 backscatter time series, including and excluding lakes and the open water fraction of the respective grid cells. These differences are caused by the considerable offsets between the thresholds for the backscatter time series including and excluding lakes used in the freeze/thaw detection algorithm (Naeimi et al., 2012) (see Fig. 6). Our results show that using time series including lakes in freeze/thaw algorithms leads, in most cases, to an early thaw date. How many days thaw is detected prior to the timing resulting from using time series excluding lakes is strongly correlated with the open water fraction of the respective ASCAT grid cell. The timing of freeze-up is mostly detected earlier when using SAR time series including water bodies, compared to using time series excluding water bodies.

A high fraction of lakes leads to comparably high backscatter in winter, closer to the summer level. This eventually leads to an earlier detection of thaw. In summer, backscatter is lower, being closer to the winter backscatter than without lakes. This leads to an earlier detection of freeze-up.

A small number of grid cells show a later freeze timing when water body areas are included and for a small number of grid cells later thaw timing is shown (see Figs. 8 and 9). For those grid cells, including water body areas in the backscatter time series leads to a stronger overestimation of the length of the thawed or the frozen period. For the majority of grid cells investigated in the study, including backscatter from water bodies in the freeze/thaw analysis does not, however, lead to an over or under estimation of the thawed or frozen period but rather

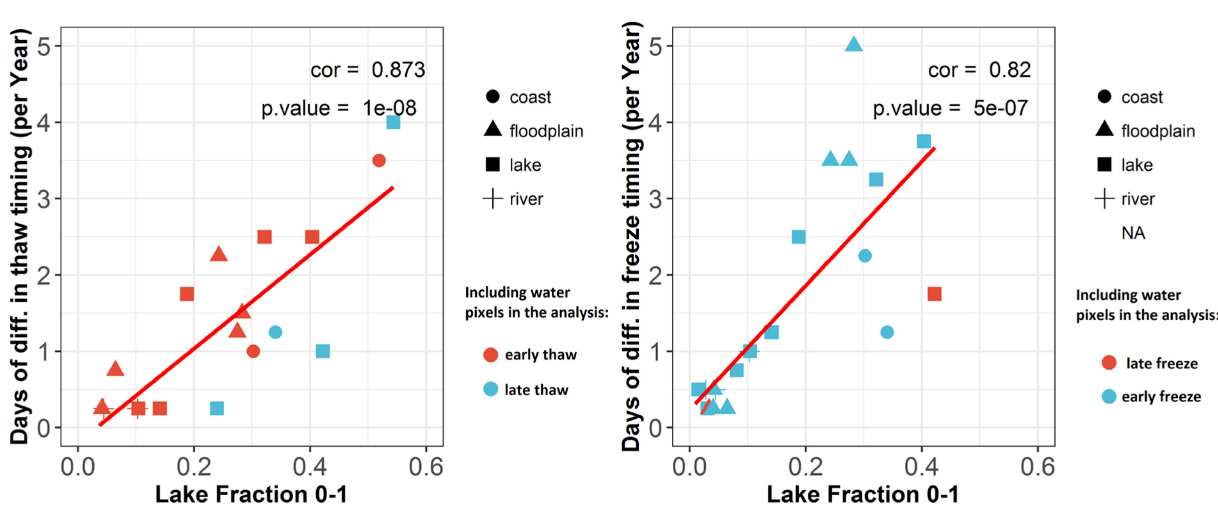

Fig. 8. Differences of freeze and thaw timing in days per year for the period 2015–2018 resulting from the Sentinel-1 time series excluding and including lakes.

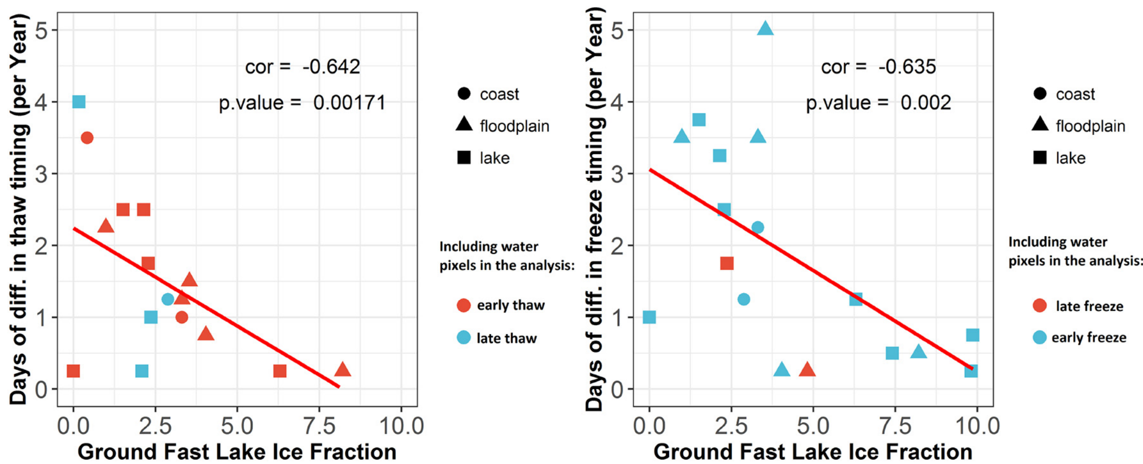

Fig. 9. Differences of freeze and thaw timing in days per year for the period 2015–2018 resulting from the Sentinel-1 time series excluding and including lakes in relationship with relative ground fast lake ice fraction per grid cell in %.

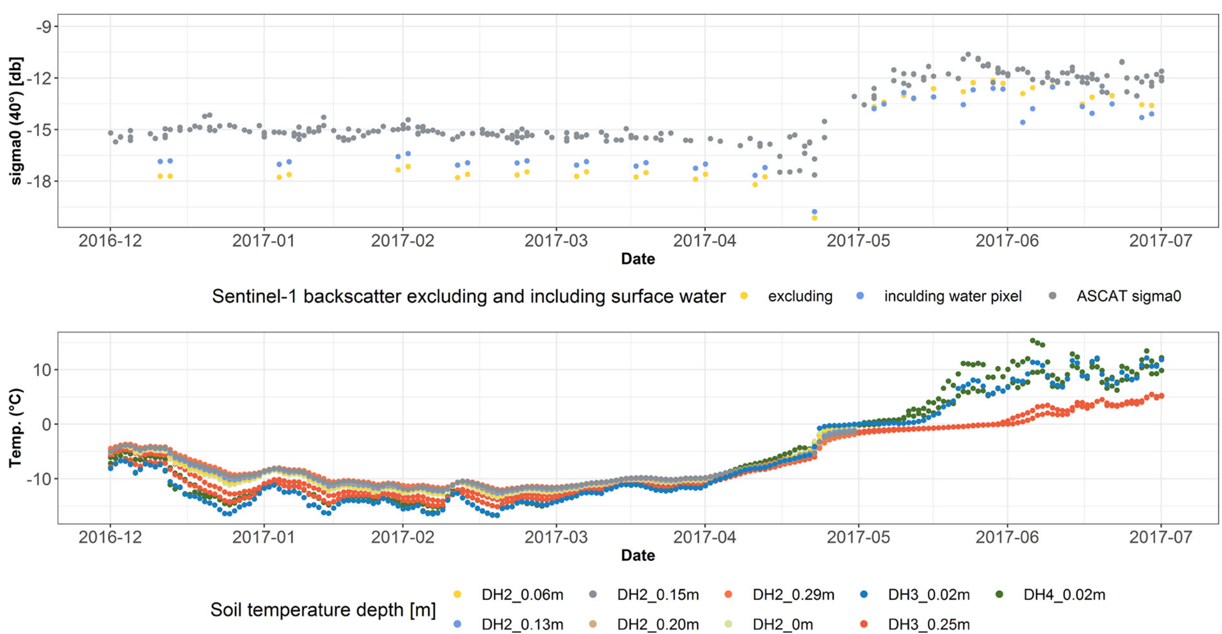

Fig. 10. Time series of ASCAT backscatter, Sentinel-1 mean values (including and excluding water pixels) and *in situ* soil temperature measurements (70.16°N, 148.48°W). All *in situ* measurements displayed here were obtained from sites within the corresponding ASCAT grid cell. *In situ* data for sites Deadhorse 2–4 obtained from the Permafrost Laboratory.

to a shift of both periods. The grid cells affected by an overestimation of the thawed or frozen period are characterized as coastal, floodplain and lake-rich areas. Grid cells including coastal waters are expected to have different behaviors from those including only inland water bodies. Variations in water level due to tidal changes or storm induced high floods may cause the water masks to be less accurate. Additionally, coastal water might introduce biases into the time series (including water pixel) that are disproportionate to the open water fraction or contrary to the influences caused by inland waters. Saline water (within the ocean or near coastal water bodies) causes a different freeze-up timing compared to adjacent freshwater that can cause mixed signals in the backscatter time series (Stewart and Platford, 1986; Anderson et al., 1999). For grid cells located within extensive floodplains it can be assumed that the created water masks are less accurate due to the dynamic behavior of these specific water bodies.

Offsets between ASCAT backscatter time series and Sentinel-1 time series excluding surface water bodies (seen in Fig. 6) are caused by the underlying offset between backscatter values of the two time series. This may be caused by a number of factors. While ASCAT and Sentinel-1 operate at the same frequency (C-band) and we limited the Sentinel-1 observations used in this study to those with VV-polarization, the sensors still have inherent differences which may contribute to the offset between the data sets. Additionally, ASCAT observations are not originally given in the gridded format but rather each observation represents a specific elliptical footprint that does not completely match with the Sentinel-1 subsets for this study. However, the main conclusions of this analysis do not rely on the direct comparison of Sentinel-1 and ASCAT but rather on the comparison of different time series created solely from Sentinel-1 observations. In this case, the issue of the mismatch of footprints and grid cell geometry becomes negligible. In addition, due to the nature of the ASCAT acquisitions, the elliptical footprint shifts slightly from acquisition to acquisition. Using the best approximation for each single footprint for the Sentinel-1 subsets would lead to differing surface water fractions between observations due to slightly different footprints.

Figs. 10, 11 and 12 show within grid cell variability of *in situ* near

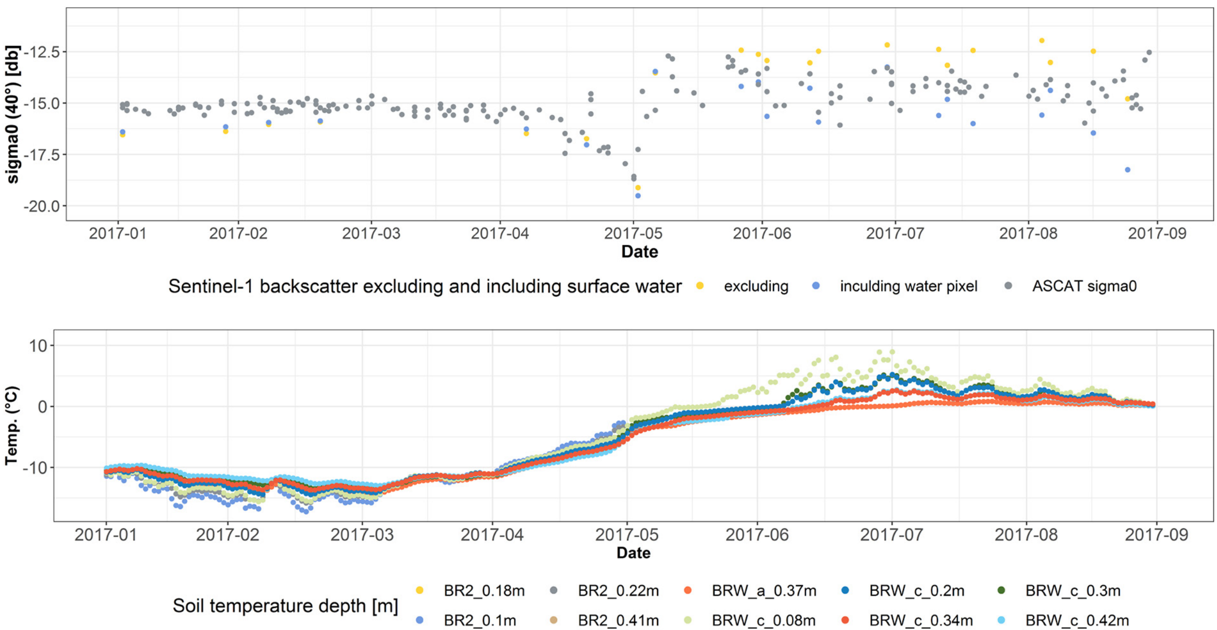

Fig. 11. Time series of ASCAT backscatter, Sentinel-1 mean values (including and excluding water pixels) and *in situ* soil temperature measurements (71.28°N, 156.67°W). All *in situ* measurements displayed here were obtained from sites within the corresponding ASCAT grid cell. *In situ* data for sites Barrow 2, A and C from the Permafrost Laboratory.

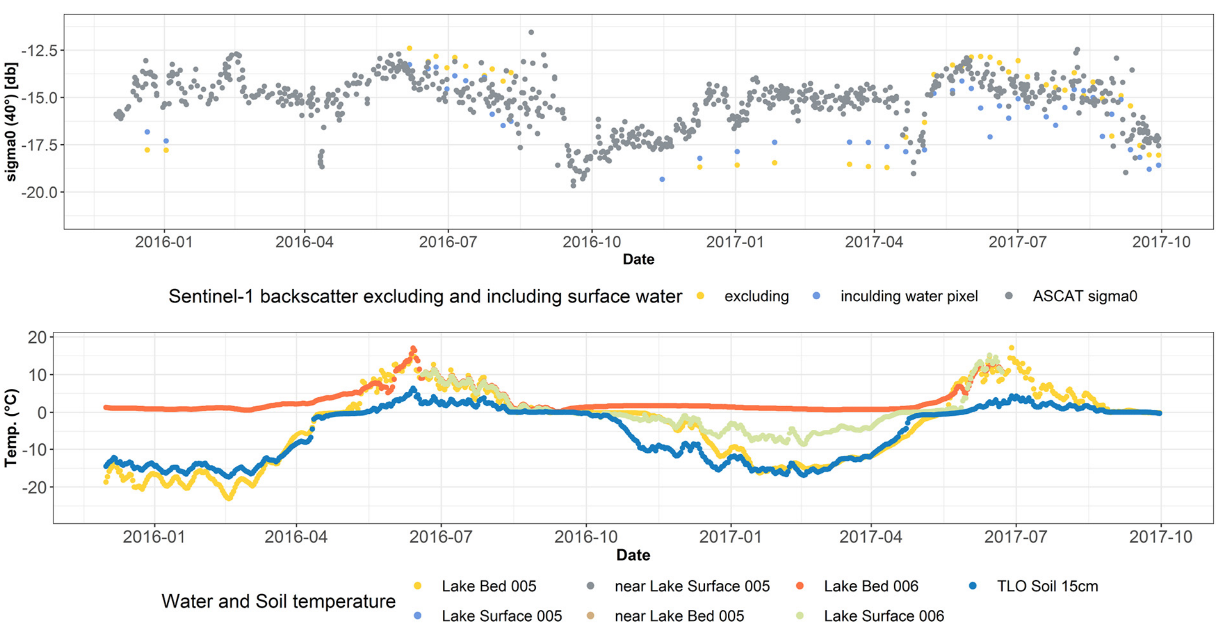

Fig. 12. Time series of ASCAT backscatter, Sentinel-1 mean values (including and excluding water pixels) and *in situ* soil temperature and water temperature measurements (71.28°N, 156.67°W). All *in situ* measurements displayed here were obtained from sites within the corresponding ASCAT grid cell. *In situ* data for sites Tes005, Tess006 and TLO (Teshekpuk Lake Observatory).

Table 3
Results of the comparison of the Sentinel-1 based freeze/thaw classification (incl. and excl. surface water) and *in situ* near-surface temperature for selected study sites including the ASCAT Grid cell ID, location and name of the study site (Kaldoaivi, TLO (Teshekpuk Lake Observatory), Barrow), available years and agreement in %.

ASCAT grid cell	Location	Site	Years	% incl	% excl.
3061839	69.83°N, 27.27°E	Kaldoaivi	2016–2018	78.8	94.84
3080728	70.72°N, 153.83°W	TLO	2015–2017	71.43	80.95
3091198	71.28°N, 156.60°W	Barrow C	2017	85.71	90.48

surface soil and *in situ* water temperatures. The heterogeneity of soil temperatures highlights a general uncertainty of coarse scale measurements. The difference in lake temperatures as visible in Fig. 12 highlights the additional heterogeneity introduced into coarse scale measurements by water bodies and suggests that a simple adjustment of freeze/thaw results using open water fraction might not account for all uncertainty introduced into scatterometer data by sub-grid cell surface water bodies. The maximum open water fraction of grid cells included in this study is 60%. It is therefore possible that areas with an even higher open water fraction than studied here will show higher offsets as reported for our chosen areas.

5.2. Special cases: rivers, coastal areas, and ground fast lake ice

Several of the study sites contain (in addition to lakes) rivers or coastal waters. Some sites containing coastal waters can be seen as outliers in Figs. 8 and 9. However, not all grid cells containing rivers or coastal waters behave as outliers in this analysis. While lakes of a certain size are generally masked in freeze/thaw products, rivers are small/narrow and therefore have mostly not been masked in previously published freeze/thaw products (Paulik et al., 2014). Including grid cells from coastal or river rich areas is important when studying the Arctic. Rivers are a common feature in arctic areas and excluding all grid cells including rivers from any analysis would lead to large gaps in resulting data sets. Coastal areas in permafrost zones are known to be important sites of erosion and dynamic changes (Günther et al., 2013; Lantuit et al., 2013; Jones et al., 2018) and can therefore not be omitted when studying freeze/thaw dynamics. In coastal and river areas, the issue of footprint and grid cell mismatch is of greater importance. Rivers and coastal waters introduce additional heterogeneity into the analysis. The additional heterogeneity in the form of different dynamics of the different types of water bodies may lead to diverse impacts on backscatter. Rivers and coastal waters both show different ice regimes compared to lakes (Magnuson et al., 2000; Michel and Ramseier, 1971). The assumption that this could lead to a stronger overall offset for these grid cells could not be corroborated by our results. This is likely due to the fact that the summer mean seems to be the parameter most influenced by the lake areas and not the freeze/thaw or snowmelt level (see Fig. 6).

The comparison of the difference of days in thaw and freeze-up with the fraction of ground fast lake ice per grid cell reveals negative correlations with lower numbers of days misclassified for higher ground fast lake ice fractions. However, as shown in Fig. 2 in our sample, grid cells with the highest ground fast lake ice fractions are those with low overall open water fractions. When taking this into account, our results do not show an impact of ground fast ice situations on the freeze/thaw retrieval. As the ground fast lake ice data set (Bartsch et al., 2017a, 2017b) is based on ASAR data from one single year (2008), it can be assumed that it does not represent the current ground fast state for all studied grid cells. This introduces additional uncertainty into this part of the results.

5.3. Uncertainties and potential error sources

The radiometric accuracy of Sentinel-1 and ASCAT observations is an important factor contributing to the validity of our results. The radiometric accuracy of Sentinel-1 has been extensively studied by Schmidt et al. (2018), among others (*e.g.* Mattia et al., 2017; Recchia et al., 2018; Torres et al., 2017). Schmidt et al. (2018) found a radiometric accuracy for the IW mode of 0.30 db for a study period of 1.5 years. This value is significantly smaller in comparison to the typical differences of backscatter observed over frozen and unfrozen ground which in this study ranged between approximately 2–4 db. It can therefore be assumed that the radiometric accuracy of Sentinel-1 backscatter is high enough for the purposes of this study. For ASCAT the radiometric accuracy has been found to be similar to Sentinel-1. Wilson et al. (2010) found an average radiometric accuracy of 0.3 db to 0.35 db.

In this study, both the scatterometer and SAR data sets were used in σ^0. The ASCAT product which was used in this study is provided in sigma0 by EUMETSAT as part of the operational soil moisture product. This is related to the fact that algorithms and data sets used in the community for freeze/thaw mapping (changes in liquid water content) are generally based on σ^0 (Bartsch et al., 2007, 2010; Naeimi et al., 2012; Park et al., 2011). The aim of this study was to assess and improve data sets and algorithms used by different research communities today. To achieve this goal, σ^0 data was used both for ASCAT and Sentinel-1, to make this work applicable and relevant for critical data sets (such as operational soil moisture and freeze thaw retrieval data sets (*e.g.* Wagner et al., 2010; Naeimi et al., 2012; Paulik et al., 2014; Baghdadi et al., 2018). Multiple studies discuss the advantages of using gamma0 data for SAR applications (*e.g.* Small et al., 2004; Wicks et al., 2018; Small, 2011). Utilizing gamma0 instead of σ^0 for Sentinel-1 data would allow for higher accuracy in mountainous areas. For future studies, or studies focusing exclusively on Sentinel-1, using data in gamma0 could be an interesting alternative.

A comparison of the water masks created for this analysis with established lake and surface water data products reveals high percentages of agreement. As the different data sets are based on data obtained at different time periods and with different spatial resolution, perfect agreements was not expected. The PeRL data set contains, in addition to lakes, small ponds that are not included in our water mask due to the resolution of Sentinel-2. Other areas of disagreement between our water mask and the established data products are mainly located at edges of lakes. These areas are highly influenced by the seasonality of Arctic water bodies as well as temporal changes in the extent of lakes which together with the different acquisition times of the data used to create the different surface water products causes the disagreement in those areas.

The accuracy of the freeze/thaw retrieval algorithm employed in this study has been extensively tested by Naeimi et al. (2012). The authors reported overall accuracies between 80.26% and 91.79% for the comparison with *in situ* soil temperature data, an overall accuracy of 81.93% for the comparison with air temperature and overall accuracies with modeled soil temperatures between 83.09% and 83.86% for ERA-Interim and GLDAS-Noah data respectively (Naeimi et al., 2012). The reported accuracy for the different data sets was different for frozen, unfrozen and transitional periods (Naeimi et al., 2012). Highest accuracy was reported for unfrozen periods (91.36% to 92.32%), followed by frozen periods (77.87% to 88.36%) and transitional periods (70.81% to 75.09%) (Naeimi et al., 2012).

Comparison of freeze/thaw classification results with *in situ* near-surface soil temperature measurements revealed high agreements from 80.95% to 94.84% for classifications based on Sentinel-1 backscatter time series excluding lakes. Classification results based on time series including lakes showed lower agreement with *in situ* data records from 71.43% to 85.71% (see Table 3). Complete agreement was not expected as we compare the freeze/thaw classification results with *in situ* point measurements which therefore do not represent the same spatial extent. The higher agreement of classification results excluding surface water compared to those including water bodies underlines our findings that surface water within grid cells negatively impacts freeze/thaw classifications in a significant way.

5.4. Potential implications for applications

The offsets between time series including and excluding lakes found in this study for Sentinel-1 time series can be assumed to be comparable to the influence surface water bodies have on coarse scatterometer data, specifically ASCAT. The comparable frequencies of the sensors on board the Sentinel-1 constellation and ASCAT (both C-band) suggest a similar response of backscatter changes to the presence of surface water bodies. Recently, circumpolar freeze/thaw data sets have been used in a variety of applied studies (*e.g.* Kroisleitner et al., 2018; Park et al., 2016). Kroisleitner et al. (2018) have applied freeze/thaw data, specifically the number of frozen days, to estimate the mean annual ground temperature on a circumpolar level. Performing these kind of analyses on the scale of the coarse spatial resolution of ASCAT grid cells allow for a circumpolar scope. However, sub-grid cell lakes have not been specifically considered. Our study clearly shows the importance of considering the open water fraction when performing analysis on the scale of scatterometer data. The linear relationship of the offset with the open water fraction suggests the possibility of a corrective function for coarse scale scatterometer based freeze/thaw data sets on the basis of the lake (or surface water) fraction. Considering the results shown in Fig. 8, grid cells with at and beyond 40% open water fraction show an offset in spring of 2 days and on offset of 3.5 days in autumn. This translates to an overestimation of the frozen season of 1.5 day per year. According to the findings by Kroisleitner et al. (2018), this would result in a 0.1 °C lower mean annual ground temperature.

Lake-rich regions in the Arctic have undergone and will further undergo responses due to climate change (Surdu et al., 2014; Arp et al., 2016; Schuur et al., 2008). An approach to account for the offset introduced by lakes and other surface waters should therefore be dynamic and incorporate the possibly changing open water fraction over time. Dynamics in lake- and river-ice break-up and freeze-up as well as the timing of these events is thought to be responsive to climate change as ice development is highly sensitive to changes in winter temperature and snow (Duguay et al., 2003; Arp et al., 2016).

6. Conclusions

This study examines the relationship of freeze/thaw data quality and sub-grid cell surface water bodies. Our findings show a significant influence of sub-grid cell water bodies on coarse scale C-band backscatter and consequently on resulting freeze/thaw data sets. The analysis reveals a disproportionate influence of the water bodies contribution to the coarse scale backscatter during the unfrozen period on the quality of the freeze/thaw results as well as the importance of backscatter contribution from water bodies during frozen and transitional periods. The comparison of the freeze/thaw classification with *in situ* soil temperature data revealed an increasing accuracy when surface water areas were omitted, underlining the importance of our results for future applications of scatterometer data to freeze/thaw retrieval.

We found a general overestimation of the number of frozen days caused by sub-grid cell surface water which increases with increasing open water fractions. The overestimation of frozen days range from 0.5 days per year to 1.5 days per year for areas with 10% and 40% surface water fraction, respectively. The results highlight the importance of considering the complex relationship of backscatter observations with sub-grid cell water bodies when creating and using freeze/thaw data products.

Declaration of Competing Interest

The authors declare that they have no known competing financial interests or personal relationships that could have appeared to influence the work reported in this paper.

Acknowledgements

This work was supported by the Austrian Science Fund (Fonds zur Förderung der wissenschaftlichen Forschung, FWF) through the Doctoral College GIScience (DK W1237–N23). It was further supported through ESA DUE GlobPermafrost (4000116196/15/I–NB) and ESA CCI + Permafrost (4000123681/18/I-NB). Benjamin M. Jones was supported by the National Science Foundation under grant OPP-1806213 and the National Fish and Wildlife Foundation under grant # 8006.19.063445. Parts of the *in situ* data used in this study was obtained through the Permafrost Laboratory (Geophysical Institute University of Alaska Fairbanks) and we would like to thank Vladimir Romanovsky for the permission to use these data sets in our analysis. The authors would like to thank Wayana Dolan (University of North Carolina at Chapel Hill) for fruitful discussion on water masks and Sentinel-2. The authors would like to thank Christopher D. Arp for providing data on lake surface and lake bottom temperatures.

References

Anderson, N.J., Bennike, O., Christoffersen, K., Jeppesen, E., Markager, S., Miller, G., Renberg, I., 1999. Limnological and palaeolimnological studies of lakes in south-western Greenland. Geol. Greenland Surv. Bull. 183, 68–74.

Arndt, K.A., Oechel, W.C., Goodrich, J.P., Bailey, B.A., Kalhori, A., Hashemi, J., Sweeney, C., Zona, D., 2019. Sensitivity of methane emissions to later soil freezing in Arctic tundra ecosystems. J. Geophys. Res. Biogeosci. 0. https://doi.org/10.1029/2019JG005242.

Arp, C.D., Jones, B.M., 2009. Geography of Alaska lake districts: identification, description, and analysis of lake-rich regions of a diverse and dynamic state. In: Technical Report U. S. Geological Survey.

Arp, C.D., Jones, B.M., Liljedahl, A.K., Hinkel, K.M., Welker, J.A., 2015. Depth, ice thickness, and ice-out timing cause divergent hydrologic responses among arctic lakes. Water Resour. Res. 51, 9379–9401. https://doi.org/10.1002/2015WR017362.

Arp, C.D., Jones, B.M., Grosse, G., Bondurant, A.C., Romanovsky, V.E., Hinkel, K.M., Parsekian, A.D., 2016. Threshold sensitivity of shallow arctic lakes and sublake permafrost to changing winter climate. Geophys. Res. Lett. 43, 6358–6365. https://doi.org/10.1002/2016GL068506.

Baghdadi, N., Bazzi, H., El Hajj, M., Zribi, M., 2018. Detection of frozen soil using sentinel-1 SAR data. Remote Sens. 10 URL: https://www.mdpi.com/2072-4292/10/8/1182. doi: 10.3390/rs10081182.

Bartalis, Z., Kidd, R., Scipal, K., 2006. Development and implementation of a Discrete Global Grid System for soil moisture retrieval using the MetOp ASCAT scatterometer. In: 1st EPS/MetOp RAO Workshop. Citeseer.

Bartsch, A., Kidd, R.A., Wagner, W., Bartalis, Z., 2007. Temporal and spatial variability of the beginning and end of daily spring freeze/thaw cycles derived from scatterometer data. Remote Sens. Environ. 106, 360–374. https://doi.org/10.1016/j.rse.2006.09.004.

Bartsch, A., Kumpula, T., Forbes, B.C., Stammler, F., 2010. Detection of snow surface thawing and refreezing in the Eurasian Arctic with QuikSCAT: implications for reindeer herding. Ecol. Appl. 20, 2346–2358 URL: https://esajournals.onlinelibrary.wiley.com/doi/abs/10.1890/09-1927.1. doi: 10.1890/09-1927.1. arXiv:https://esajournals.onlinelibrary.wiley.com/doi/pdf/10.1890/09-1927.1.

Bartsch, A., Höfler, A., Kroisleitner, C., Trofaier, A.M., 2016. Land cover mapping in northern high latitude permafrost regions with satellite data: achievements and remaining challenges. Remote Sens. 8. https://doi.org/10.3390/rs8120979.

Bartsch, A., Pointner, G., Leibman, M.O., Dvornikov, Y., Khomutov, A.V., Trofaier, A.M., 2017a. Circumpolar ground-fast lake ice fraction by lake from ENVISAT ASAR late winter 2008, links to Shapfiles. doi: 10.1594/PANGAEA.873674 supplement to: Bartsch, A et al. (2017): Circumpolar Mapping of Ground-Fast Lake Ice. Front. Earth Sci. 5 (12). https://doi.org/10.3389/feart.2017.00012. (16 pp.).

Bartsch, A., Pointner, G., Leibman, M.O., Dvornikov, Y.A., Khomutov, A.V., Trofaier, A.M., 2017b. Circumpolar mapping of ground-fast Lake ice. Front. Earth Sci. 5, 1–16. https://doi.org/10.3389/feart.2017.00012.

Bartsch, A., Leibman, M., Strozzi, T., Khomutov, A., Widhalm, B., Babkina, E., Mullanurov, D., Ermokhina, K., Kroisleitner, C., Bergstedt, H., 2019. Seasonal progression of ground displacement identified with satellite radar interferometry and the impact of unusually warm conditions on permafrost at the Yamal peninsula in 2016. Remote Sens. 11, 1865.

Bauer-Marschallinger, B., Paulik, C., Hochstöger, S., Mistelbauer, T., Modanesi, S., Ciabatta, L., Massari, C., Brocca, L., Wagner, W., 2018. Soil moisture from fusion of scatterometer and sar: closing the scale gap with temporal filtering. Remote Sens. 10. https://doi.org/10.3390/rs10071030.

Bergstedt, H., Bartsch, A., 2017. Surface state across scales; temporal and spatial patterns in land surface freeze/thaw dynamics. Geosciences 7, 65.

Bergstedt, H., Bartsch, A., 2020. Near Surface Ground Temperature, Soil Moisture and Snow Depth Measurements in the Kaldoaivi Wilderness Area, for 2016–2018. URL:. https://doi.org/10.1594/PANGAEA.912482.

Bergstedt, H., Zwieback, S., Bartsch, A., Leibman, M., 2018. Dependence of C-band backscatter on ground temperature, air temperature and snow depth in Arctic permafrost regions. Remote Sens. 10. https://doi.org/10.3390/rs10010142.

Cai, X., Feng, L., Hou, X., Chen, X., 2016. Remote sensing of the water storage dynamics of large lakes and reservoirs in the yangtze river basin from 2000 to 2014. Sci. Rep. 6, 36405.

Carroll, M., Wooten, M., DiMiceli, C., Sohlberg, R., Kelly, M., 2016. Quantifying surface water dynamics at 30 meter spatial resolution in the north american high northern latitudes 1991–2011. Remote Sens. 8. https://doi.org/10.3390/rs8080622.

Dee, D.P., Uppala, S.M., Simmons, A.J., Berrisford, P., Poli, P., Kobayashi, S., Andrae, U., Balmaseda, M.A., Balsamo, G., Bauer, P., Bechtold, P., Beljaars, A.C.M., van de Berg, L., Bidlot, J., Bormann, N., Delsol, C., Dragani, R., Fuentes, M., Geer, A.J., Haimberger, L., Healy, S.B., Hersbach, H., Hólm, E.V., Isaksen, L., Kållberg, P., Köhler, M., Matricardi, M., McNally, A.P., Monge-Sanz, B.M., Morcrette, J.-J., Park, B.-K., Peubey, C., de Rosnay, P., Tavolato, C., Thépaut, J.-N., Vitart, F., 2011. The era-interim reanalysis: configuration and performance of the data assimilation system. Q. J. R. Meteorol. Soc. 137, 553–597. https://doi.org/10.1002/qj.828.

Derksen, C., Xu, X., Dunbar, R.S., Colliander, A., Kim, Y., Kimball, J.S., Black, T.A., Euskirchen, E., Langlois, A., Loranty, M.M., Marsh, P., Rautiainen, K., Roy, A., Royer, A., Stephens, J., 2017. Retrieving landscape freeze/thaw state from Soil Moisture Active Passive (SMAP) radar and radiometer measurements. Remote Sens. Environ. 194, 48–62. https://doi.org/10.1016/j.rse.2017.03.007.

Dobson, M.C., Ulaby, F.T., 1986. Active microwave soil moisture research. IEEE Trans. Geosci. Remote Sens. GE-24, 23–36. https://doi.org/10.1109/TGRS.1986.289585.

Du, Y., Zhang, Y., Ling, F., Wang, Q., Li, W., Li, X., 2016. Water bodies€™ mapping from sentinel-2 imagery with modified normalized difference water index at 10-m spatial

resolution produced by sharpening the SWIR band. Remote Sens. 8. https://doi.org/10.3390/rs8040354.
Duguay, C., Rouse, W., Lafleur, P., Boudreau, L., Crevier, Y., Pultz, T., 1999. Analysis of multi-temporal ERS-1 SAR data of subarctic tundra and forest in the northern Hudson Bay lowland and implications for climate studies. Can. J. Remote. Sens. 25, 21–33. https://doi.org/10.1080/07038992.1999.10855260.
Duguay, C.R., Pultz, T.J., Lafleur, P.M., Drai, D., 2002. RADARSAT backscatter characteristics of ice growing on shallow sub-Arctic lakes, Churchill, Manitoba, Canada. Hydrol. Process. 16, 1631–1644. https://doi.org/10.1002/hyp.1026.
Duguay, C.R., Flato, G.M., Jeffries, M.O., Ménard, P., Morris, K., Rouse, W.R., 2003. Ice-cover variability on shallow lakes at high latitudes: model simulations and observations. Hydrol. Process. 17, 3465–3483. https://doi.org/10.1002/hyp.1394.
Engram, M., Arp, C.D., Jones, B.M., Ajadi, O.A., Meyer, F.J., 2018. Analyzing floating and bedfast lake ice regimes across Arctic Alaska using 25 years of space-borne SAR imagery. Remote Sens. Environ. 209, 660–676. https://doi.org/10.1016/j.rse.2018.02.022.
Figa-Saldaña, J., Wilson, J.J., Attema, E., Gelsthorpe, R., Drinkwater, M., Stoffelen, A., 2002. The advanced scatterometer (ASCAT) on the meteorological operational (MetOp) platform: a follow on for European wind scatterometers. Can. J. Remote. Sens. 28, 404–412.
Frauenfeld, O.W., Zhang, T., Mccreight, J.L., 2007. Northern Hemisphere freezing/thawing index variations over the twentieth century. Int. J. Climatol. 27, 47–63. https://doi.org/10.1002/joc.1372.
Frolking, S., McDonald, K.C., Kimball, J.S., Way, J., Zimmermann, R., Running, S.W., 1999. Using the space-borne NASA scatterometer (NSCAT) to determine the frozen and thawed seasons. J. Geophys. Res.-Atmos. 104, 27895–27907.
Gascon, F., Cadau, E., Colin, O., Hoersch, B., Isola, C., Fernández, B.L., Martimort, P., 2014. Copernicus Sentinel-2 mission: products, algorithms and cal/val. In: Earth Observing Systems XIX (p. 92181E). International Society for Optics and Photonics. 9218.
Geudtner, D., Torres, R., Snoeij, P., Davidson, M., Rommen, B., 2014. Sentinel-1 system capabilities and applications. In: 2014 IEEE Geoscience and Remote Sensing Symposium, pp. 1457–1460. https://doi.org/10.1109/IGARSS.2014.6946711.
Green, J., Kongoli, C., Prakash, A., Sturm, M., Duguay, C., Li, S., 2012. Quantifying the relationships between lake fraction, snow water equivalent and snow depth, and microwave brightness temperatures in an arctic tundra landscape. Remote Sens. Environ. 127.
Grosse, G., Jones, B., Arp, C., 2013. Thermokarst lakes, drainage, and drained basins. In: Shroder, J.F. (Ed.), Treatise on Geomorphology. Elsevier, Amsterdam, Netherlands, pp. 325–353.
Günther, F., Overduin, P.P., Sandakov, A.V., Grosse, G., Grigoriev, M.N., 2013. Short- and long-term thermo-erosion of ice-rich permafrost coasts in the Laptev Sea region. Biogeosciences 10, 4297–4318. https://doi.org/10.5194/bg-10-4297-2013.
Hahn, S., Reimer, C., Vreugdenhil, M., Melzer, T., Wagner, W., 2017. Dynamic characterization of the incidence angle dependence of backscatter using MetOp ASCAT. IEEE J. Select. Topics Appl. Earth Observ. Rem. Sens. 10, 2348–2359.
Hallikainen, M., Ulaby, F., Dobson, M., El-Rayes, M., 1984. Dielectric measurements of soils in the 3 to 37 GHz band between 50° C and 23° C. ESA IGARSS 84. Rem. Sens. 1.
Högström, E., Bartsch, A., 2017. Impact of backscatter variations over water bodies on coarse-scale radar retrieved soil moisture and the potential of correcting with meteorological data. IEEE Trans. Geosci. Remote Sens. 55, 3–13.
Högström, E., Trofaier, A.M., Gouttevin, I., Bartsch, A., 2014. Assessing seasonal backscatter variations with respect to uncertainties in soil moisture retrieval in Siberian tundra regions. Remote Sens. 6, 8718–8738. https://doi.org/10.3390/rs6098718.
Jiang, Z., Huete, A.R., Chen, J., Chen, Y., Li, J., Yan, G., Zhang, X., 2006. Analysis of ndvi and scaled difference vegetation index retrievals of vegetation fraction. Remote Sens. Environ. 101, 366–378. https://doi.org/10.1016/j.rse.2006.01.003.
Jones, B.M., Farquharson, L.M., Baughman, C.A., Buzard, R.M., Arp, C.D., Grosse, G., Bull, D.L., Günther, F., Nitze, I., Urban, F., et al., 2018. A decade of remotely sensed observations highlight complex processes linked to coastal permafrost bluff erosion in the arctic. Environ. Res. Lett. 13, 115001.
Kim, Y., Kimball, J.S., McDonald, K.C., Glassy, J., 2011. Developing a global data record of daily landscape freeze/thaw status using satellite passive microwave remote sensing. IEEE Trans. Geosci. Remote Sens. 49, 949–960. https://doi.org/10.1109/TGRS.2010.2070515.
Kim, Y., Kimball, J.S., Glassy, J., Du, J., 2017. An extended global earth system data record on daily landscape freeze–thaw status determined from satellite passive microwave remote sensing. Earth Syst. Sci. Data 9, 133–147. https://doi.org/10.5194/essd-9-133-2017.
Kimball, J., McDonald, K., Keyser, A., Frolking, S., Running, S., 2001. Application of the NASA Scatterometer (NSCAT) for determining the daily frozen and nonfrozen landscape of Alaska. Remote Sens. Environ. 75, 113–126. https://doi.org/10.1016/S0034-4257(00)00160-7.
Kimball, J., McDonald, K., Frolking, S., Running, S., 2004. Radar remote sensing of the spring thaw transition across a boreal landscape. Remote Sens. Environ. 89, 163–175. https://doi.org/10.1016/j.rse.2002.06.004. (BOREAS Remote Sensing Science).
Kontu, A., Kemppainen, S., Lemmetyinen, J., Pulliainen, J., Hallikainen, M., 2008. Determination of snow emission on lake ice from airborne passive microwave measurements. In: IGARSS 2008–2008 IEEE International Geoscience and Remote Sensing Symposium. 4https://doi.org/10.1109/IGARSS.2008.4779905. (pp. IV – 1046–IV – 1049).
Kroisleitner, C., Bartsch, A., Bergstedt, H., 2018. Circumpolar patterns of potential mean annual ground temperature based on surface state obtained from microwave satellite data. Cryosphere 12, 2349–2370. https://doi.org/10.5194/tc-12-2349-2018.
Kutser, T., Paavel, B., Verpoorter, C., Ligi, M., Soomets, T., Toming, K., Casal, G., 2016. Remote sensing of black lakes and using 810 nm reflectance peak for retrieving water quality parameters of optically complex waters. Remote Sens. 8. https://doi.org/10.3390/rs8060497.
Lantuit, H., Overduin, P.P., Wetterich, S., 2013. Recent progress regarding permafrost coasts. Permafr. Periglac. Process. 24, 120–130. https://doi.org/10.1002/ppp.1777.
Lehner, B., Döll, P., 2004. Development and validation of a global database of lakes, reservoirs and wetlands. J. Hydrol. 296, 1–22. https://doi.org/10.1016/j.jhydrol.2004.03.028.
Magnuson, J.J., Robertson, D.M., Benson, B.J., Wynne, R.H., Livingstone, D.M., Arai, T., Assel, R.A., Barry, R.G., Card, V., Kuusisto, E., Granin, N.G., Prowse, T.D., Stewart, K.M., Vuglinski, V.S., 2000. Historical trends in lake and river ice cover in the northern hemisphere. Science 289, 1743–1746. https://doi.org/10.1126/science.289.5485.1743.
Mastepanov, M., Sigsgaard, C., Dlugokencky, E.J., Houweling, S., Ström, L., Tamstorf, M.P., Christensen, T.R., 2008. Large tundra methane burst during onset of freezing. Nature 456, 628–630. https://doi.org/10.1038/nature07464.
Matgen, P., Heitz, S., Hasenauer, S., Hissler, C., Brocca, L., Hoffmann, L., Wagner, W., Savenije, H., 2012. On the potential of MetOp ASCAT-derived soil wetness indices as a new aperture for hydrological monitoring and prediction: a field evaluation over Luxembourg. Hydrol. Process. 26, 2346–2359.
Mattia, F., Balenzano, A., Satalino, G., Lovergine, F., Loew, A., Peng, J., Wegmuller, U., Santoro, M., Cartus, O., Dabrowska-Zielinska, K., Musial, J., Davidson, M.W.J., Yueh, S., Kim, S., Das, N., Colliander, A., Johnson, J., Ouellette, J., Walker, J., Wu, X., McNairn, H., Merzouki, A., Powers, J., Caldwell, T., Entekhabi, D., Cosh, M., Jackson, T., 2017. Sentinel-1 high resolution soil moisture. In: 2017 IEEE International Geoscience and Remote Sensing Symposium (IGARSS), pp. 5533–5536. https://doi.org/10.1109/IGARSS.2017.8128257.
McDonald, K. C., & Kimball, J. S. (2006). Estimation of surface freeze–thaw states using microwave sensors. In Encyclopedia of Hydrological Sciences. John Wiley & Sons, Ltd. URL: https://doi.org/10.1002/0470848944.hsa059a. doi: https://doi.org/10.1002/0470848944.hsa059a.
McFeeters, S.K., 1996. The use of the Normalized Difference Water Index (NDWI) in the delineation of open water features. Int. J. Remote Sens. 17, 1425–1432.
Michel, B., Ramseier, R., 1971. Classification of river and lake ice. Can. Geotech. J. 8, 36–45.
Muster, S., Roth, K., Langer, M., Lange, S., Cresto-Aleina, F., Bartsch, A., Morgenstern, A., Grosse, G., Jones, B., Sannel, A.B.K., Sjöberg, Y., Günther, F., Andresen, C., Veremeeva, A., Lindgren, P.R., Bouchard, F., Lara, M.J., Fortier, D., Charbonneau, S., Virtanen, T.A., Hugelius, G., Palmtag, J., Siewert, M.B., Riley, W.J., Koven, C.D., Boike, J., 2017. PeRL: Permafrost Region Pond and Lake Database, links to ArcGIS shapefiles. URL: 10.1594/PANGAEA.868349. doi: 10.1594/PANGAEA.868349 supplement to: Muster, S et al. (2017): PeRL: a circum-Arctic Permafrost Region Pond and Lake database. Earth Syst. Sci. Data 9 (1), 317–348. https://doi.org/10.5194/essd-9-317-2017.
Naeimi, V., Scipal, K., Bartalis, Z., Hasenauer, S., Wagner, W., 2009. An improved soil moisture retrieval algorithm for ERS and METOP scatterometer observations. IEEE Trans. Geosci. Remote Sens. 47, 1999–2013.
Naeimi, V., Paulik, C., Bartsch, A., Wagner, W., Kidd, R., Park, S.E., Elger, K., Boike, J., 2012. ASCAT surface state flag (SSF): extracting information on surface freeze/thaw conditions from backscatter data using an empirical threshold-analysis algorithm. IEEE Trans. Geosci. Remote Sens. 50, 2566–2582. https://doi.org/10.1109/TGRS.2011.2177667.
Nitze, I., Grosse, G., Jones, B.M., Romanovsky, V.E., Boike, J., 2018. Remote sensing quantifies widespread abundance of permafrost region disturbances across the arctic and subarctic. Nat. Commun. 9, 5423.
Park, S.-E., Bartsch, A., Sabel, D., Wagner, W., Naeimi, V., Yamaguchi, Y., 2011. Monitoring freeze/thaw cycles using envisat asar global mode. Remote Sens. Environ. 115, 3457–3467. https://doi.org/10.1016/j.rse.2011.08.009.
Park, H., Kim, Y., Kimball, J.S., 2016. Widespread permafrost vulnerability and soil active layer increases over the high northern latitudes inferred from satellite remote sensing and process model assessments. Remote Sens. Environ. 175, 349–358. https://doi.org/10.1016/j.rse.2015.12.046.
Pathe, C., Wagner, W., Sabel, D., Doubkova, M., Basara, J.B., 2009. Using envisat asar global mode data for surface soil moisture retrieval over oklahoma, usa. IEEE Trans. Geosci. Remote Sens. 47, 468–480. https://doi.org/10.1109/TGRS.2008.2004711.
Paulik, C., Melzer, T., Hahn, S., Bartsch, A., Heim, B., Elger, K., Wagner, W., 2014. Circumpolar Surface Soil Moisture and Freeze/Thaw Surface Status Remote Sensing Products (Version 4) with Links to Geotiff Images and NetCDF Files (2007–01 to 2013–12). https://doi.org/10.1594/PANGAEA.832153.
Pekel, J.-F., Cottam, A., Gorelick, N., Belward, A.S., 2016. High-resolution mapping of global surface water and its long-term changes. Nature 540, 418.
Pithan, F., Mauritsen, T., 2014. Arctic amplification dominated by temperature feedbacks in contemporary climate models. Nat. Geosci. 7, 181–184. https://doi.org/10.1038/ngeo2071.
Pointner, G., Bartsch, A., Forbes, B.C., Kumpula, T., 2018. The role of lake size and local phenomena for monitoring ground-fast lake ice. Int. J. Remote Sens. 0, 1–27. https://doi.org/10.1080/01431161.2018.1519281.
Polishchuk, Y.M., Bogdanov, A.N., Polishchuk, V.Y., Manasypov, R.M., Shirokova, L.S., Kirpotin, S.N., Pokrovsky, O.S., 2017. Size distribution, surface coverage, water, carbon, and metal storage of Thermokarst lakes in the permafrost zone of the Western Siberia lowland. Water 9. https://doi.org/10.3390/w9030228.
Rautiainen, K., Parkkinen, T., Lemmetyinen, J., Schwank, M., Wiesmann, A., Ikonen, J., Derksen, C., Davydov, S., Davydova, A., Boike, J., et al., 2016. SMOS prototype algorithm for detecting autumn soil freezing. Remote Sens. Environ. 180, 346–360.
Recchia, A., Giudici, D., Piantanida, R., Miranda, N., Guarnieri, A.M., 2018. Sentinel-l radiometric accuracy enhancement exploiting antenna model refinement technique. In: IGARSS 2018–2018 IEEE International Geoscience and Remote Sensing

Symposium, pp. 6360–6363. https://doi.org/10.1109/IGARSS.2018.8519050.
Rees, A., English, M., Dersken, C., Walker, A., Duguay, C., 2006. Uncertainty in snow mass retrievals from passive microwave sensor data in lake-rich high latitude environments. Hydrol. Process. 20 URL: http://onlinelibrary.wiley.com/doi/10.1002/hyp.6076/abstract.
Rignot, E., Way, J.B., 1994. Monitoring freeze—thaw cycles along North-South Alaskan transects using ERS-1 SAR. Remote Sens. Environ. 49, 131–137. https://doi.org/10.1016/0034-4257(94)90049-3.
Romanovsky, V., Cable, W., Kholodov, A., 2015. Changes in permafrost and active-layer temperature along an Alaskan permafrost-ecological transect. In: 68th Canadian geotechnical conference and 7th Canadian permafrost conference. 2015. GEOQubec, pp. 68.
Sabel, D., Park, S.-E., Bartsch, A., Schlaffer, S., Klein, J.-P., Wagner, W., 2012. Regional Surface Soil Moisture and Freeze/Thaw Timing Remote Sensing Products With Links to Geotiff Images. https://doi.org/10.1594/PANGAEA.779658.
Schmidt, K., Ramon, N.T., Schwerdt, M., 2018. Radiometric accuracy and stability of sentinel-1A determined using point targets. Int. J. Microw. Wirel. Technol. 10, 538–546.
Schuur, E.A.G., Bockheim, J., Canadell, J.G., Euskirchen, E., Field, C.B., Goryachkin, S.V., Hagemann, S., Kuhry, P., Lafleur, P.M., Lee, H., Mazhitova, G., Nelson, F.E., Rinke, A., Romanovsky, V.E., Shiklomanov, N., Tarnocai, C., Venevsky, S., Vogel, J.G., Zimov, S.A., 2008. Vulnerability of permafrost carbon to climate change: implications for the global carbon cycle. BioScience 58, 701–714. https://doi.org/10.1641/B580807.
Showstack, R., 2014. Sentinel satellites initiate new era in earth observation. EOS Trans. Am. Geophys. Union 95, 239–240. https://doi.org/10.1002/2014EO260003.
Small, D., 2011. Flattening gamma: radiometric terrain correction for SAR imagery. IEEE Trans. Geosci. Remote Sens. 49, 3081–3093.
Small, D., Meier, E., Nuesch, D., 2004. Robust radiometric terrain correction for SAR image comparisons. In: IGARSS 2004. 2004 IEEE International Geoscience and Remote Sensing Symposium. 3. pp. 1730–1733 volume 3.
Smith, L.C., Sheng, Y., MacDonald, G.M., 2007. A first pan-Arctic assessment of the influence of glaciation, permafrost, topography and peatlands on northern hemisphere lake distribution. Permafr. Periglac. Process. 18, 201–208. https://doi.org/10.1002/ppp.581.
Stewart, K.M., Platford, R.F., 1986. Hypersaline gradients in two Canadian High Arctic lakes. Can. J. Fish. Aquat. Sci. 43, 1795–1803.
Surdu, C.M., Duguay, C.R., Brown, L.C., Fernández Prieto, D., 2014. Response of ice cover on shallow lakes of the North Slope of Alaska to contemporary climate conditions (1950-2011): radar remote-sensing and numerical modeling data analysis. Cryosphere 8, 167–180. https://doi.org/10.5194/tc-8-167-2014.
Surdu, C.M., Duguay, C.R., Pour, H.K., Brown, L.C., 2015. Ice freeze-up and break-up detection of shallow lakes in northern Alaska with spaceborne SAR. Remote Sens. 7, 6133–6159. https://doi.org/10.3390/rs70506133.
Torres, R., Navas-Traver, I., Bibby, D., Lokas, S., Snoeij, P., Rommen, B., Osborne, S., Ceba-Vega, F., Potin, P., Geudtner, D., 2017. Sentinel-1 SAR system and mission. In: 2017 IEEE Radar Conference (RadarConf), pp. 1582–1585. https://doi.org/10.1109/RADAR.2017.7944460.
Ulaby, F.T., Batlivala, P.P., Dobson, M.C., 1978. Microwave backscatter dependence on surface roughness, soil moisture, and soil texture: part I-bare soil. IEEE Trans. Geosci. Electron. 16, 286–295. https://doi.org/10.1109/TGE.1978.294586.
Ulaby, F.T., Dubois, P.C., Van Zyl, J., 1996. Radar mapping of surface soil moisture. J. Hydrol. 184, 57–84.
Wagner, W., Bartalis, Z., Naeimi, V., Park, S., Figa-Saldaña, J., Bonekamp, H., 2010. Status of the Metop ASCAT soil moisture product. In: 2010 IEEE International Geoscience and Remote Sensing Symposium, pp. 276–279.
Wang, G., Hu, H., Li, T., 2009. The influence of freeze–thaw cycles of active soil layer on surface runoff in a permafrost watershed. J. Hydrol. 375, 438–449. https://doi.org/10.1016/j.jhydrol.2009.06.046.
Wegmüller, U., 1990. The effect of freezing and thawing on the microwave signatures of bare soil. Remote Sens. Environ. 33, 123–135. https://doi.org/10.1016/0034-4257(90)90038-N.
Wicks, D., Jones, T., Rossi, C., 2018. Testing the interoperability of sentinel-1 analysis ready data over the United Kingdom. In: IGARSS 2018–2018 IEEE International Geoscience and Remote Sensing Symposium, pp. 8655–8658.
Widhalm, B., Bartsch, A., Goler, R., 2018. Simplified normalization of C-band synthetic aperture radar data for terrestrial applications in high latitude environments. Remote Sens. 10. https://doi.org/10.3390/rs10040551.
Wilson, J., Anderson, C., Baker, M., Bonekamp, H., Saldana, J.F., Dyer, R., Lerch, J., Kayal, G., Gelsthorpe, R., Brown, M., et al., 2010. Radiometric calibration of the advanced wind scatterometer radar ASCAT carried onboard the METOP-A satellite. IEEE Trans. Geosci. Remote Sens. 48, 3236–3255.
Woo, M., 1986. Permafrost hydrology in North America. Atmosphere-Ocean 24, 201–234. https://doi.org/10.1080/07055900.1986.9649248.
Woo, M.-K., Winter, T.C., 1993. The role of permafrost and seasonal frost in the hydrology of northern wetlands in North America. J. Hydrol. 141, 5–31. https://doi.org/10.1016/0022-1694(93)90043-9. Introduction to the 28th International Geological Congress Symposium on the Hydrogeology of Wetlands.
Zhang, T., Armstrong, R.L., 2001. Soil freeze/thaw cycles over snow-free land detected by passive microwave remote sensing. Geophys. Res. Lett. 28, 763–766. https://doi.org/10.1029/2000GL011952.
Zhang, T., Barry, R.G., Armstrong, R.L., 2004. Application of satellite remote sensing techniques to frozen ground studies. Polar Geogr. 28, 163–196. https://doi.org/10.1080/789610186.
Zhang, Y., Chen, W., Riseborough, D.W., 2008. Transient projections of permafrost distribution in Canada during the 21st century under scenarios of climate change. Glob. Planet. Chang. 60, 443–456. https://doi.org/10.1016/j.gloplacha.2007.05.003.
Zhao, S., Zhang, L., Zhang, T., Hao, Z., Chai, L., Zhang, Z., 2012. An empirical model to estimate the microwave penetration depth of frozen soil. In: Geoscience and Remote Sensing Symposium (IGARSS), 2012 IEEE International. IEEE, pp. 4493–4496.